JACS Au
AN OPEN ACCESS JOURNAL OF THE AMERICAN CHEMICAL SOCIETY

pubs.acs.org/jacsau
Article

High-Performance Mixed-Matrix Membranes Using a Zeolite@MOF Core−Shell Structure Synthesized via Ion-Exchange-Induced Crystallization and Post-Synthetic Conversion

Hye Leen Choi, Yeanah Jeong, Hongju Lee, and Tae-Hyun Bae*

Cite This: JACS Au 2024, 4, 253−262
Read Online

ACCESS | Metrics & More | Article Recommendations | Supporting Information

ABSTRACT: Strategic design of nanostructures, such as the core−shell configuration, offers a promising avenue to harness the desired properties while mitigating the inherent limitations of individual materials. In our pursuit of synergizing the advantages of two distinct porous materials, namely, zeolites and metal−organic frameworks (MOFs), we aimed to develop the zeolite@MOF core−shell structures. To synthesize this targeted material while minimizing undesirable side reactions, we devised an innovative approach involving ion-exchange-induced crystallization and post-synthetic conversion. This method enabled the exclusive growth of a MOF on the zeolite surface. Specifically, we successfully crafted a CaA@ZIF-8 core−shell structure, employing it in the fabrication of mixed-matrix membranes for CO_2 separation. Within this core−shell configuration, the ZIF-8 in the shell played a crucial role in enhancing the filler−polymer interfaces, leading to the development of defect-free membranes. Simultaneously, the CaA zeolite core exhibited a highly selective transport of CO_2. The synergistic effects resulted in a membrane incorporating a CaA@ZIF-8 core−shell filler, which demonstrated a high CO_2 permeability of 1142 Barrer and a CO_2/CH_4 selectivity of 43.3, significantly surpassing the established upper limits for polymeric membranes. Our findings underscore the potential of core−shell structures composed of microporous materials for achieving the coveted properties necessary for high-performance gas separation membranes.

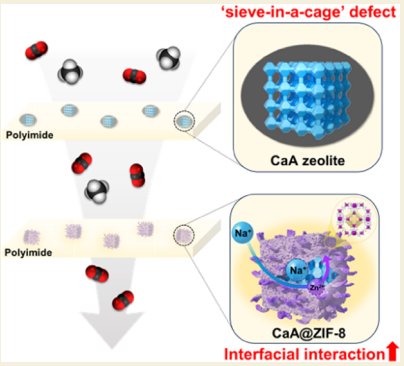

KEYWORDS: *zeolite, metal−organic framework, zeolite−MOF core−shell, mixed-matrix membranes, gas separation*

1. INTRODUCTION

Given the substantial increase in atmospheric carbon dioxide (CO_2) emissions and the demand for clean energy production, there is an increasing focus on technologies that can efficiently separate CO_2 from gas mixtures.[1] These technologies are relevant for various applications, such as biogas upgrading, hydrogen purification, and postcombustion carbon capture.[2,3] In these applications, membrane-based gas separation has garnered significant attention due to its numerous advantages, such as low energy consumption, operational simplicity, and compact design.[4] Although polymeric membranes have been widely employed in gas separation applications, there has been a strong focus on enhancing their performance beyond that of conventional polymer membranes. This has led to extensive research on mixed-matrix membranes (MMMs) in recent years, which consist of a combination of a polymer matrix and microporous filler.[5−13] MMMs capitalize on the beneficial characteristics of the polymer matrix, including its high processability and mechanical stability, while also leveraging the exceptional separation capabilities offered by microporous filler materials. As a result, a diverse range of porous materials have been investigated as potential fillers for MMMs.

Zeolites, such as LTA, have been utilized as fillers in MMMs for CO_2 separation due to their advantageous attributes, including long-term stability, reasonable cost, and remarkable molecular sieving properties stemming from their rigid pore structures.[10,11] Nonetheless, the fabrication of MMMs presents certain challenges. One such challenge is the occurrence of the "sieve-in-a-cage" defect, which arises from the weak interfacial compatibility between the organic matrix and the inorganic filler. This defect creates a bypass pathway around the filler, allowing gas molecules to pass rapidly through a nonselective route without interacting with the filler material, resulting in subpar separation performance.[14−17] In contrast, metal−organic frameworks (MOFs) have been developed and gained attention due to their large pore volumes and adjustable functionality.[18,19] While the high synthesis cost and poor stability of MOFs have hindered their widespread practical application, some stable and cost-effective MOFs have been synthesized for gas separation processes. For instance, ZIF-8 has been employed as a filler material in the fabrication of CO_2-selective MMMs.[8] ZIF-8 possesses well-defined pore

Received: November 2, 2023
Revised: December 22, 2023
Accepted: January 2, 2024
Published: January 11, 2024

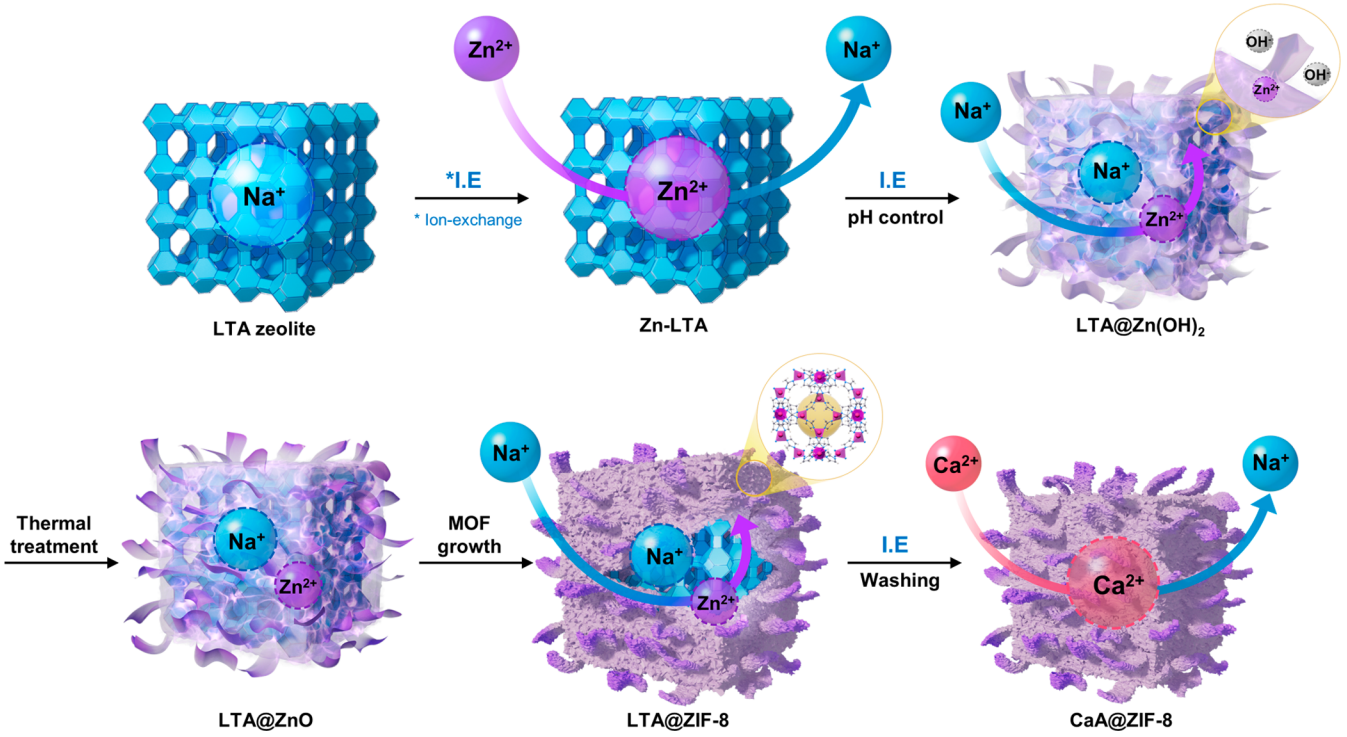

Figure 1. Schematic illustration of the synthesis process for CaA@ZIF-8 core−shell composites.

channels that facilitate the rapid transport of CO_2 molecules, leading to enhanced CO_2 permeability in the resulting MMMs.[20] More importantly, the organic component of ZIF-8 aids in improving the interfaces between the filler and polymer, thereby mitigating the formation of interfacial defects. However, it should be noted that the CO_2 selectivity of ZIF-8 is inferior to that of the CaA (Ca-exchanged LTA) zeolite, which has been proven to possess a high selectivity for CO_2 molecules.

As an effort to combine the advantages of two different kinds of materials, nanomaterials have often been synthesized in core−shell hybrid structures. MOFs have been extensively used to design such a hybrid structure. In membrane-based gas separation area, the core−shell structured filler materials such as MOF-mesoporous silica,[21,22] MOF-graphene oxide,[23] MOF-carbon nanotube,[24] and MOF−MOF[25,26] have been explored to fabricate MMMs. However, to the best of our knowledge, the zeolite−MOF core−shell structure has not yet been used for the fabrication of the MMM thus far. We believe zeolite@MOF core−shell structure can offer several potential benefits and synergistic effects, which lead to an enhancement in gas separation performance of resulting MMMs. For example, to design high-performance MMMs for CO_2 separation, the ZIF-8, which possesses a high gas permeability and a good affinity to polymer matrices, can be used as the shell material. Meanwhile, CaA zeolite, which can selectively adsorb and transport CO_2, can be employed as the core material. Such CaA@ZIF-8 filler material can enhance both CO_2 permeability and selectivity while forming a good filler/polymer interface owing to good compatibility between the MOF and polymer.

Numerous investigations have been conducted concerning the synthesis of zeolite@MOF core−shell composites.[27−29] The commonly employed technique involves seeded growth, wherein a presynthesized core material (zeolite) is introduced into the mother solution for the shell material (MOF) synthesis before the reaction initiation. Despite its effectiveness in achieving complete coverage of the core material's surface, controlling the morphology of the shell layer remains a challenge. Furthermore, throughout the reaction duration, the potential arises for the formation of pure MOF material in the bulk phase alongside the intended core−shell composite, thus giving rise to undesired mixtures.

To overcome the aforementioned limitations of conventional methods, we introduce a novel approach for fabricating zeolite@MOF core−shell structures, illustrated in Figure 1. This innovative technique capitalizes on the reversible ion-exchange property of zeolite, enabling the targeted formation of metal hydroxide nanowhiskers exclusively on the zeolite surface, as showcased in our prior research endeavors.[30] Subsequently, these nanowhiskers undergo seamless conversion into MOF through post-synthetic transformation processes. In this study, we successfully engineered the CaA@ZIF-8 core−shell architecture. Further, we accomplished the production of high-quality MMMs incorporating this core−shell filler and polyimides, exhibiting negligible filler−polymer interfacial defects. Through systematic adjustments of filler loading and polymer matrices, we finely tuned the CO_2 separation performance, resulting in a remarkable CO_2/CH_4 separation capability that significantly surpasses the upper bound of conventional polymeric membranes.

2. RESULTS AND DISCUSSION

2.1. Synthesis and Morphological Evolution to Zeolite@MOF Core−Shell Structure

The procedural sequence and corresponding structural transformation of CaA@ZIF-8 core−shell composites are illustrated in Figure 1. The initial step involved the introduction of Zn^{2+} ions into the LTA through an ion-exchange process. Subsequently, this Zn-LTA material was exposed to a mildly basic aqueous solution containing Na^+. As a result of the

https://doi.org/10.1021/jacsau.3c00680
JACS Au 2024, 4, 253−262

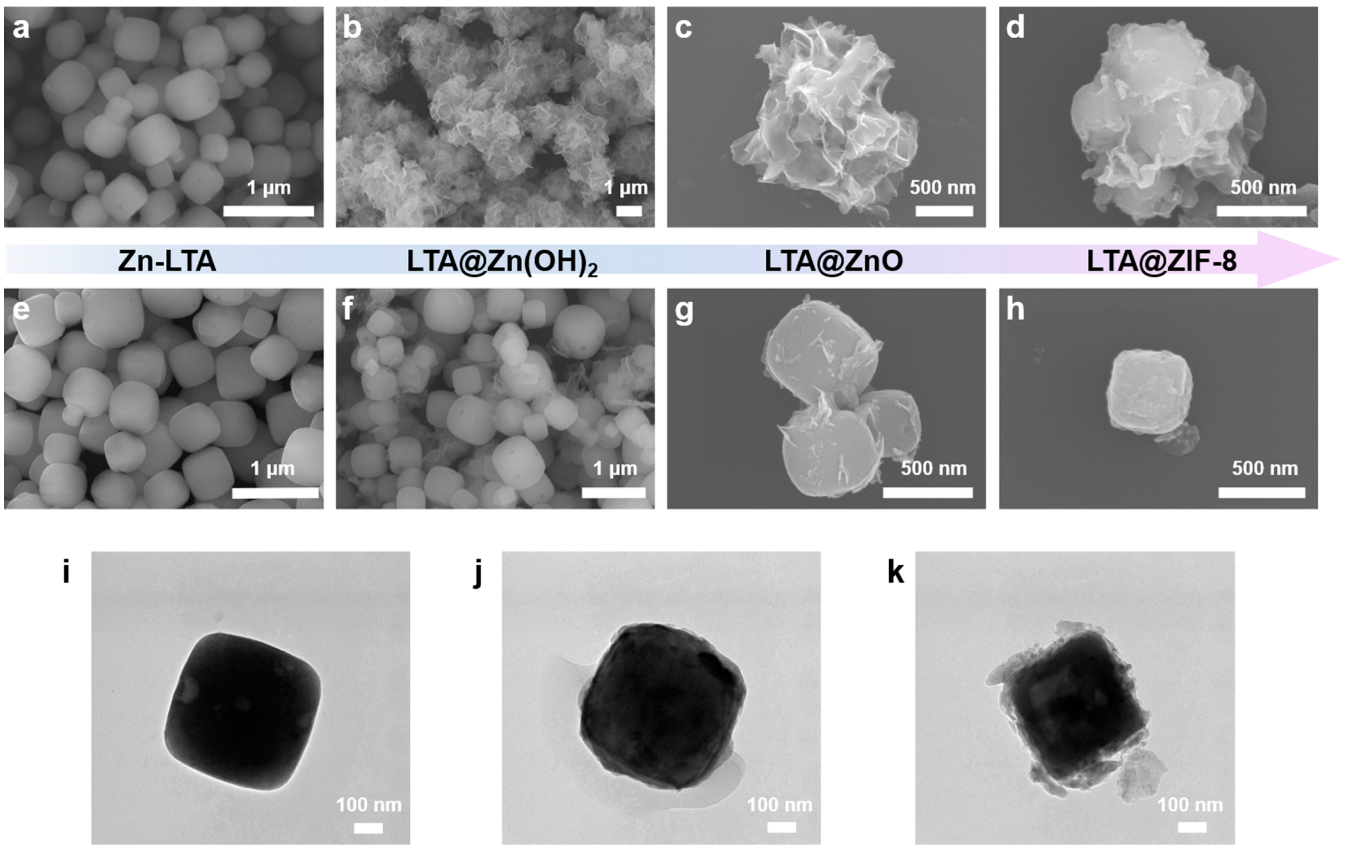

Figure 2. FE-SEM and TEM images of nanoparticles. (a, e) FE-SEM images of Zn-LTAX, (b, f) LTAX@$Zn(OH)_2$, (c, g) LTAX@ZnO, and (d, h) LTAX@ZIF-8 nanoparticles; (a–d) for X = 100 and (e–h) for X = 50. (i) TEM images of CaA, (j) CaA50@ZIF-8, and CaA100@ZIF-8 nanoparticles.

reversible ion-exchange mechanism, Zn^{2+} ions were displaced and subsequently reacted with hydroxyl ions (OH^-) available in the weakly basic solution (with a pH of 9.5), leading to the formation of $Zn(OH)_2$ nanowhiskers on the surfaces of the zeolite. A subsequent thermal treatment was conducted to convert $Zn(OH)_2$ into ZnO, as a metal oxide is preferred as a precursor for MOF conversion over metal hydroxides. Following this, the ZnO nanowhiskers were transformed into ZIF-8 in the presence of 2-methylimidazole linker. Notably, Na^+ ions were introduced during this step as ion-exchange promoters, aiding in the extraction of any residual Zn^{2+} ions that might remain within the zeolite. This synthesis pathway offers a distinct advantage by enabling the growth of MOF exclusively on the zeolite surface, facilitated by the zeolite's reversible ion-exchange properties that provide a source of metal ions. Lastly, an ion exchange was executed using Ca^{2+} ions to enhance the permeability of the filler as well as its CO_2 sorption capacity, leading to the formation of a CaA zeolite.

After synthesizing LTA@ZnO, we conducted thermal gravimetric analysis (TGA) to rapidly assess the materials' microporosity. Figure S3 reveals that except for LTA50@ZnO, all other variants displayed no weight loss. This indicates that ZnO, formed on the zeolite, effectively blocked the zeolite's pores. Typically, LTA zeolite possesses hydrophilic properties and readily absorbs moisture, resulting in weight loss due to moisture loss up to 200 °C, as illustrated by the black line. In contrast, LTAX@ZnO (X = 100, 95, 90, 80, and 75) did not exhibit this phenomenon, confirming that ZnO formation on the surface obstructed the zeolite's pores. Visual confirmation of significantly reduced ZnO loading in LTA50@ZnO, which has the lowest degree of ion exchange, is presented in Figure S2. Therefore, when the Zn^{2+}-exchange degree is too high (resulting in excessive ZnO formation), the surface coverage by ZnO increases but simultaneously leads to pore blockage in the zeolite. Conversely, when the Zn^{2+}-exchange degree is low (resulting in lower ZnO formation), the zeolite's pores are preserved. For the upcoming comparison of the two types of fillers, we focused on Zn-LTA100, which possesses the highest degree of Zn^{2+}-exchange, and Zn-LTA50, which is characterized by the lowest degree of Zn^{2+}-exchange.

Figure 2 presents scanning electron microscopy (SEM) images depicting the stepwise synthesis of LTA@ZIF-8 core–shell fillers. Figure 2a,e shows the smooth surfaces of Zn-LTA, which were unchanged from the original LTA crystal, as shown in Figure S1. In Figure 2b,f, it is evident that nanowhisker-shaped $Zn(OH)_2$ has grown on the surface of the zeolite for both LTA50@$Zn(OH)_2$ and LTA100@$Zn(OH)_2$. This morphology was preserved even after the conversion from $Zn(OH)_2$ to ZnO. As the degree of Zn^{2+}-exchange increased, the amount of $Zn(OH)_2$ growth on the surface also increased. Consequently, LTA50@$Zn(OH)_2$ exhibits relatively nonuniform surface coverage by $Zn(OH)_2$ due to a lower degree of Zn^{2+}-exchange. However, TEM images in Figure 2i–k illustrate that CaA50@ZIF-8 features a thin ZIF-8 shell with a thickness of several tens of nanometers on the smooth surface of the LTA zeolite. In contrast, a more roughened surface was observed for LTA100@ZIF-8 compared to LTA50@ZIF-8, owing to the larger amount of the $Zn(OH)_2$ whisker structure in the intermediate stage.

https://doi.org/10.1021/jacsau.3c00680
JACS Au 2024, 4, 253–262

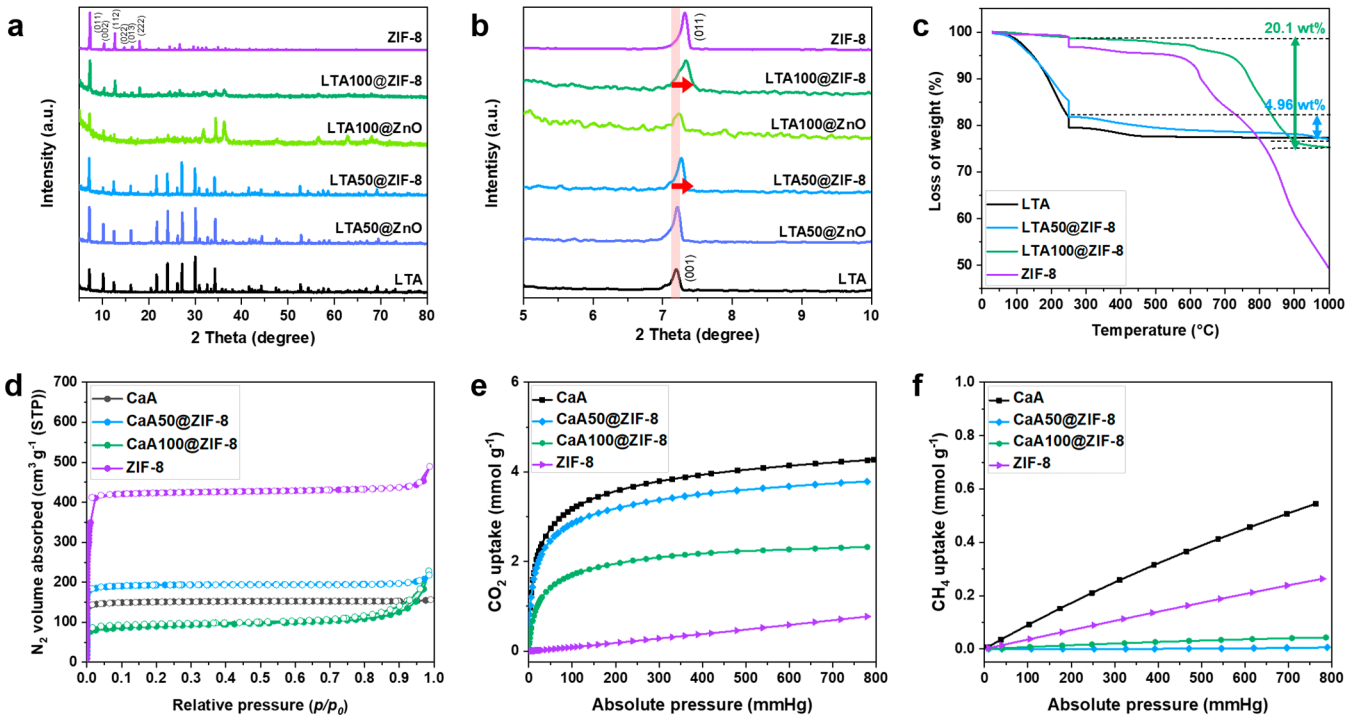

Figure 3. (a) XRD patterns of LTA, ZIF-8, LTA@ZnO, and LTAX@ZIF-8 (X = 100, 50) nanoparticles. (b) Enlargement of XRD patterns at low degree regions. (c) TGA curves of fillers. (d) N_2 physisorption isotherms of fillers at 77 K. Enclosed circles represent adsorption, and open circles represent desorption. (e) CO_2 and (f) CH_4 single component adsorption isotherm at 25 °C.

2.2. Characterizations of the Core−Shell Fillers

X-ray diffraction (XRD) analysis was conducted to confirm the conversion of LTA@ZnO to LTA@ZIF-8, as shown in Figure 3a,b. Both LTA and ZIF-8 possess a sodalite structure, which leads to the presence of signature peaks at similar positions, posing a challenge for analysis. However, the transformation of ZnO to ZIF-8 was confirmed by the protrusion of peaks at 7.4° (011), 10.4° (002), 12.7° (112), 14.7° (022), 16.4° (013), and 18.0° (222).[31] This phenomenon was more prominent in LTA100@ZIF-8 compared to LTA50@ZIF-8 due to the larger amount of ZnO that had converted to ZIF-8. Similarly, peaks originating from ZnO at 31.9, 34.4, 36.3, 56.6, 63.1, and 68.1° disappeared in LTA@ZIF-8, further confirming the successful conversion of ZnO nanowhiskers grown on the zeolite surface into ZIF-8 (Figure S5). It should be noted that the lower loading amounts of ZIF-8 in LTA50@ZIF-8 made it more challenging to discern the change from LTA50@ZnO. However, upon closer examination of the 5−10° region, a slight shift was observed, with the first peak transitioning from 7.2° (001) to 7.4° (011) as ZIF-8 was formed. Consequently, all of these results collectively indicate that both LTA100@ZnO and LTA50@ZnO have successfully undergone conversion to LTA@ZIF-8.

Quantitative determination of the ZIF-8 loading was achieved through TGA curves, as illustrated in Figure 3c. The weight loss observed up to 250 °C primarily resulted from the removal of guest molecules (e.g., water vapor) from the sample pores. To eliminate the influence of these guest molecules, a controlled TGA analysis was conducted, where the ramping process was paused and the temperature was held at 250 °C for 30 min to completely eliminate moisture from the samples. Given the high thermal stability of both LTA and ZIF-8 crystals under N_2, the core−shell composites exhibited thermal stability up to 600 °C. The weight loss occurring between 600 and 1000 °C was attributed to the decomposition of ZIF-8, which includes 2-methylimidazole as the organic linker.[32] Therefore, based on the fact that the final residue consists of LTA@ZnO, the ZIF-8 loading was calculated to be 29.1 wt % for LTA100@ZIF-8 and 8.6 wt % for LTA50@ZIF-8. It is noteworthy that the curve for LTA100@ZIF-8 does not exhibit a decrease at 250 °C. As previously described in Section 2.1, this is attributed to the excessive amount of Zn^{2+} ion exchange, which led to the zeolite's pores being obstructed by a substantial quantity of ZnO.

Figure 3d presents N_2 sorption isotherms obtained at 77 K for CaA, ZIF-8, and CaA@ZIF-8 core−shell materials. The isotherm shapes of all samples exhibit the characteristic behavior of microporous materials, known as the Type I model. Subsequently, surface areas and pore volumes were calculated based on the isotherm data, and the results are summarized in Table 1. The N_2 adsorption amounts and pore volumes for CaA and ZIF-8 were found to be consistent with values reported elsewhere.[10,33] Among the samples, CaA100@ZIF-8 displays reduced pore volume and surface area compared to CaA due to the zeolite pore blockage, as mentioned previously. The reduction in the quantity of CaA

Table 1. Textural Properties of CaA, ZIF-8, and CaA@ZIF-8 Nanoparticles Calculated from N_2 Physisorption at 77 K

sample	S_{BET} [a] [$m^2\ g^{-1}$]	S_{micro} [b] [$m^2\ g^{-1}$]	V_{micro} [b] [$cm^3\ g^{-1}$]	V_{total} [c] [$cm^3\ g^{-1}$]
CaA	499	498	0.236	0.238
CaA50@ZIF-8	653	652	0.300	0.312
CaA100@ZIF-8	309	269	0.124	0.238
ZIF-8	1421	1397	0.646	0.686

[a]Determined at P/P_0 = 0.05−0.2. [b]Calculated using t-plot method micropore analysis. [c]Calculated at P/P_0 = 0.99.

https://doi.org/10.1021/jacsau.3c00680
JACS Au 2024, 4, 253−262

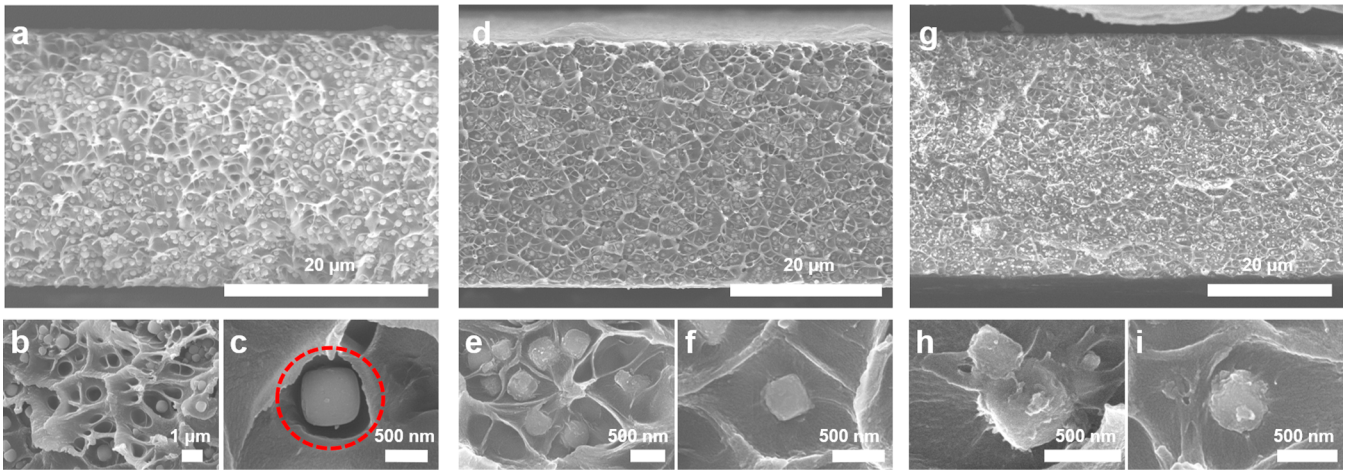

Figure 4. Cross-sectional SEM images of mixed-matrix membranes with 20 wt % filler loading. (a) Matrimid/CaA membranes at low and (b, c) high magnification. (d) Matrimid/CaA50@ZIF-8 membranes at low and (e, f) high magnification. (g) Matrimid/CaA100@ZIF-8 membranes at low and (h, i) high magnification.

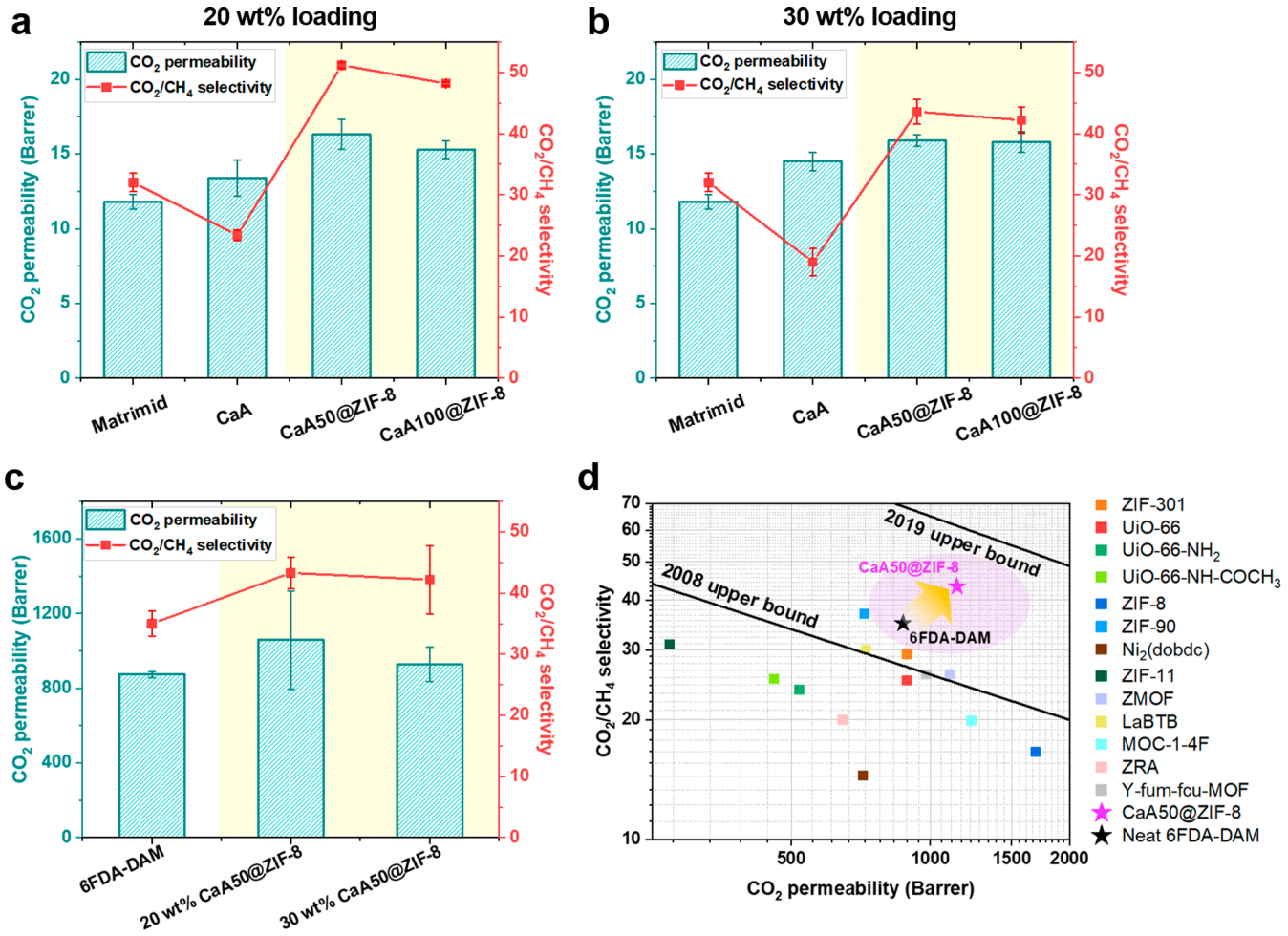

Figure 5. (a) Gas permeation properties of Matrimid-based membranes at 25 °C and 1 bar with a CO_2/CH_4 (50:50) mixture for 20 and (b) 30 wt % filler loading. (c) Gas permeation properties of 6FDA-DAM-based membranes at 25 °C and 1 bar with a CO_2/CH_4 (50:50) mixture. (d) Robeson plot for CO_2/CH_4 separation of 6FDA-DAM-based membranes with different fillers.

pores was further confirmed by the pore size distribution presented in Figure S6. Considering that the ZIF-8 loading is 29.1 wt %, it can be inferred that zeolite pores are partially obstructed, as the N_2 adsorption quantity and pore volume exceed values expected solely from the ZIF-8 content in the core−shell structure. Conversely, in the case of CaA50@ZIF-8, the N_2 adsorption amount surpasses that of CaA. Consequently, the micropore volume and Brunauer−Emmett−Teller (BET) surface area increase from 0.236 to 0.300 $cm^3\ g^{-1}$ and from 499 to 653 $m^2\ g^{-1}$, respectively. These findings

https://doi.org/10.1021/jacsau.3c00680
JACS Au 2024, 4, 253−262

suggest that the CaA50@ZIF-8 sample is a promising candidate for mixed-matrix membrane fabrication.

2.3. Gas Adsorption Properties of the Core−Shell Fillers

To explore the gas adsorption characteristics of the core−shell filler materials, we conducted measurements of CO_2 and CH_4 adsorption isotherms at 25 °C. As depicted in Figure 3e, ZIF-8 exhibited remarkably low CO_2 adsorption at 1 bar, despite its considerable surface area (1421 m^2 g^{-1}). Conversely, CaA zeolite demonstrated a high adsorption capacity, particularly in the low-pressure region, owing to its strong affinity for CO_2. Both core−shell composite materials displayed intermediate adsorption capacities, aligning with our expectations. In particular, CaA100@ZIF-8, comprising 29.1 wt % ZIF-8, exhibited a substantial reduction in CO_2 uptake compared to pristine CaA (4.23 mmol g^{-1}), resulting in a CO_2 uptake of 2.32 mmol g^{-1} at 1 bar. This value notably fell below the predicted CO_2 uptake (3.23 mmol g^{-1}), calculated based on the CaA fraction in the core−shell material. This suggests the possibility of partial pore blockage, as discussed in Section 2.2. On the other hand, CaA50@ZIF-8 demonstrated a CO_2 adsorption of 3.79 mmol g^{-1} at 1 bar, which closely approached the predicted value (3.93 mmol g^{-1}).

Figure 3f illustrates the CH_4 adsorption isotherms at 25 °C, indicating significantly reduced values in comparison to the values of the CO_2 adsorption isotherms for all samples under the same conditions. As anticipated, CaA displayed greater CO_2/CH_4 selectivity than ZIF-8. Notably, we observed the effective suppression of CH_4 adsorption within the CaA@ZIF-8 core−shell materials, at least within the parameters of our measurement conditions (limited to a sorption rate of 1.0 mbar min^{-1} using an iSorbHP1 instrument). This suppression can be attributed to the partial obstruction of CaA pores by the ZIF-8 layer formed on the surface. Nevertheless, the substantially lower CH_4 capacity values relative to the CO_2 capacity in the core−shell samples underscore the effectiveness of the CaA@ZIF-8 core−shell composite as a filler for CO_2/CH_4 separation membranes.

2.4. Fabrications of Membranes and Their Gas Permeation Properties

Cross-sectional SEM images of the mixed-matrix membranes are listed in Figure 4. Commercial Matrimid was employed as the polymer matrix for the membrane fabrication. The CaA containing membrane exhibits noticeable gaps around the fillers, forming what is commonly referred to as a "sieve-in-a-cage" morphology. This phenomenon arises due to inadequate polymer−filler adhesion, a well-documented issue in previous studies.[30,34,35] As previously mentioned, zeolites possess hydrophilic surfaces, while organic polymers tend to be hydrophobic, resulting in poor compatibility between the two. These filler−polymer interfacial defects can serve as nonselective pathways for gas molecules, reducing CO_2/CH_4 selectivity. In contrast, membranes containing CaA@ZIF-8 core−shell fillers exhibit improved polymer−filler compatibility with no discernible defects at the interfaces. This enhancement can be attributed to the organic linker in ZIF-8, which demonstrates a superior affinity with organic polymers. The mechanical property data further corroborated these findings (Figure S9 and Table S3). Membranes containing CaA@ZIF-8 core−shell fillers exhibited greater mechanical strength than membranes containing pristine CaA, which demonstrated poor polymer−filler adhesion.

Subsequently, we investigated the gas separation properties of mixed-matrix membranes based on Matrimid. Permeation testing was conducted using a binary mixture of CO_2/CH_4 (50:50) at 25 °C and 1 bar, and the results are summarized in Figure 5 and Table S4. Membranes containing CaA zeolite exhibited decreased CO_2/CH_4 selectivity due to the presence of defects at the filler−polymer interfaces. For instance, when the filler loading was 20 wt %, the CO_2/CH_4 selectivity decreased from 32.0 to 23.4 in comparison to a pure Matrimid membrane. In contrast, ZIF-8 proved highly effective in enhancing the CO_2 permeability and demonstrated the highest CO_2 permeability among all of the tested membranes, primarily due to its substantial surface area and pore volume. However, the selectivity remained relatively unchanged compared to a pure Matrimid membrane. It is important to note that the effective pore diameter of ZIF-8 is too large to achieve CO_2 and CH_4 separation through molecular sieving, as reported elsewhere.[36,37] Additionally, as discussed in Section 2.3, the sorption selectivity of ZIF-8 is inherently limited.

In contrast to the CaA and ZIF-8 fillers, the CaA@ZIF-8 core−shell fillers demonstrated a remarkable ability to simultaneously enhance both permeability and selectivity, resulting in an appealing membrane performance. Specifically, when the loading of CaA50@ZIF-8 was 20 wt %, CO_2 permeability increased from 11.8 to 16.3 Barrer compared to a pure polymeric membrane, representing a notable 38% improvement. Furthermore, the CO_2/CH_4 selectivity also increased by 37%, reaching a value of 51.2. This performance enhancement in the desired direction can be attributed to the synergistic effect of the two distinct materials comprising the core−shell structure. ZIF-8 on the shell exhibits high gas permeability and possesses a strong affinity for the organic polymer matrix, thereby inhibiting the formation of filler−polymer interfacial gaps. However, mixed-matrix membranes incorporating CaA100@ZIF-8 exhibited a lower CO_2/CH_4 selectivity compared to those containing CaA50@ZIF-8. This discrepancy can be ascribed to the observed partial pore blockage in CaA100@ZIF-8, as discussed earlier. Nevertheless, the decrease in the CO_2 permeability for membranes containing CaA100@ZIF-8 was marginal. This can be attributed to the creation of a larger quantity of ZIF-8, which possesses higher permeability than CaA, effectively compensating for the partial pore blockage in CaA. In an effort to further enhance performance, we increased the filler loading to 30%. However, no positive effect was observed with the increased filler loading. This may be attributed to nonideal factors such as filler aggregation within the matrix or minor interfacial gaps resulting from increased stress at the filler−polymer interfaces. Such postulation is further corroborated by an examination of the mechanical properties of the mixed-matrix membranes. As depicted in Figure S9 and detailed in Table S3, the membranes loaded with 30 wt % core−shell fillers displayed reduced mechanical strength compared to those with 20 wt % loading. This observation suggests that the adhesion between the polymer and filler may weaken when the filler loading exceeds a certain threshold. It is noteworthy that the ion exchange of LTA@ZIF-8 with Ca^{2+} to form CaA@ZIF-8 is necessary to achieve a high CO_2/CH_4 selectivity, as illustrated in Table S5. As mentioned in the Introduction Section, CaA exhibits high CO_2/CH_4 selectivity due to the presence of strong CO_2 binding sites within its framework.

While the use of commercial Matrimid allowed us to systematically study the effects of individual fillers, it became

https://doi.org/10.1021/jacsau.3c00680
JACS Au 2024, 4, 253−262

apparent that achieving high separation performance was challenging, as the performance of mixed-matrix membranes is primarily influenced by the properties of the continuous phase, namely, the polymer matrix.[38] In pursuit of designing a high-performance CO_2/CH_4 separation membrane, we turned to our in-house 6FDA-DAM polyimide, known for its significantly higher permeability compared to Matrimid, owing to its elevated fractional free volume.[39] To realize this goal, we employed the optimized filler, CaA50@ZIF-8. Once again, membranes containing 20 wt % filler loading exhibited marked improvements in both CO_2 permeability and CO_2/CH_4 selectivity when compared to a pure 6FDA-DAM membrane. In fact, the CO_2 permeability and CO_2/CH_4 selectivity reached exceptional values of 1142 Barrer and 43.3, respectively, surpassing the upper bound established for polymer membranes in 2008 by a significant margin. However, similar to Matrimid-based membranes, no further enhancement was observed when the loading was increased to 30%.

Lastly, we benchmarked our optimized membranes containing CaA@ZIF-8 fillers against the literature data to demonstrate the exceptional qualities of our filler material. To effectively compare the filler's performance, we sought to eliminate the influence of the polymer matrix and collected CO_2/CH_4 separation properties of 6FDA-DAM-based mixed-matrix membranes reported in the literature.[40−51] As depicted in Figure 5d and detailed in Table S6, our membrane outperforms all 6FDA-DAM-based mixed-matrix membranes containing single-phase fillers in terms of CO_2 separation properties. As previously emphasized, this remarkable enhancement can be attributed to the synergistic effect resulting from the combination of ZIF-8 and CaA zeolite, forming the core−shell structure. In summary, our gas permeation results provide strong evidence that our CaA@ZIF-8 core−shell structure is an exceptional material for designing high-performance CO_2 separation membranes.

3. CONCLUSIONS

In summary, we have pioneered the utilization of a zeolite@MOF core−shell structure in the development of mixed-matrix membranes tailored for CO_2 separation. Specifically, we have synthesized CaA@ZIF-8 core−shell structures using an innovative method involving ion-exchange-induced crystallization and post-synthetic conversion. This method allows for the exclusive growth of MOF on the zeolite surface, enabling precise control over the shell layer's morphology while minimizing undesirable side reactions. The nanoscale ZIF-8 within the shell enhances the CO_2 permeability and improves the compatibility between the filler and polymer due to the organic linker constituting the ZIF-8 framework. Simultaneously, the CaA zeolite in the core imparts exceptional selectivity for CO_2 transport, thanks to its strong affinity for CO_2 molecules. As a result of these synergistic effects, membranes composed of the CaA@ZIF-8 core−shell structure and optimized polymer exhibit remarkable performance, with a CO_2 permeability of 1142 Barrer and a CO_2/CH_4 selectivity of 43.3. These values significantly surpass the established upper limits for polymeric membranes. This study introduces an innovative synthetic strategy for zeolite@MOF fillers, which can contribute to the creation of defect-free membranes. Moreover, the proposed structural approach utilizing two distinct microporous materials holds promise for designing high-performance gas separation membranes. It is also important to note that the strategy we have outlined can be extended to other zeolite−MOF pairs for use in separating various gas pairs. Furthermore, our membrane, fabricated through the conventional solution casting technique, can ultimately undergo processing into an asymmetric structure or thin-film composite membrane, which is a practical configuration for industrial applications.

4. EXPERIMENTAL SECTION

4.1. Materials

Zinc chloride ($ZnCl_2$), sodium nitrate ($NaNO_3$), calcium nitrate tetrahydrate ($Ca(NO_3)_2{\cdot}4H_2O$), sodium hydroxide (NaOH), 2-methylimidazole (2-Mim), 2,4,6-trimethyl-1,3-diaminobenzene (DAM), 3-methylpyridine (β-picoline), and acetic anhydride (Ac_2O) were purchased from Sigma-Aldrich. 4,4′-(hexafluoroisopropylidene) diphthalic anhydride (6FDA), 1-methyl-2-pyrrolidinone (NMP), dimethylformamide (DMF), and dichloromethane (DCM) were purchased from Tokyo Chemical Industry (TCI). Methanol was obtained from Samchun Chemicals. 6FDA and DAM were purified by sublimation and dried under vacuum overnight. NMP and Ac_2O were dehydrated with molecular sieves prior to use.

4.2. Preparation of Zn^{2+}-Exchanged LTA Zeolites

The LTA zeolite (LTA), sized between 300 and 500 nm, was synthesized using the methodology outlined in prior research.[35] Following this, LTA (1.0 g) was evenly dispersed within an aqueous $ZnCl_2$ solution (50 mL) and subsequently stirred under room temperature conditions. The extent of Zn^{2+} ion exchange was tabulated in Table S1, correlating to variations in the $ZnCl_2$ solution concentration and the duration of stirring. The particles were retrieved using vacuum filtration, subjected to thorough washing with deionized water, and thereafter dried at 60 °C in a convection oven overnight. Denoted in accordance with the degree of Zn^{2+} ion exchange (X), the Zn^{2+}-exchanged zeolites were labeled as Zn-LTAX (X = 100, 95, 90, 80, 75, 50).

4.3. Synthesis of LTA@ZnO

In the standard synthesis procedure, a quantity of Zn-LTA (1.0 g) was meticulously dispersed within a 0.1 M solution of aqueous $NaNO_3$ (100 mL), with the solution's pH subsequently adjusted to 9.5 through the incorporation of NaOH. For Zn-LTA100, 95, 90, 80, and 75, the mixture was then transferred into a PTFE jar, securely sealed using Teflon tape and a cover, and heated at 90 °C for a duration of 12 h. In the case of Zn-LTA50, the process necessitated transferring the mixture into a Teflon-lined autoclave and subjecting it to heating at 160 °C for 12 h. To enhance the conversion to $Zn(OH)_2$, we intentionally adjusted the reaction conditions for Zn-LTA50, considering its relatively low degree of Zn^{2+}-exchange. Following this, the LTA@$Zn(OH)_2$ particles underwent repeated centrifugation, rigorous washing with deionized water, and eventual drying at 60 °C in a convection oven overnight. Ultimately, to transform $Zn(OH)_2$ formed on the zeolite surface into ZnO, a thermal treatment was executed at 700 °C for a duration of 2 h under ambient air conditions.[52]

4.4. Conversion to LTA@ZIF-8

The ligand solution was prepared by dissolving 2-Mim (2.05 g) in DMF (125 mL). In a round-bottom flask, LTA@ZnO (1.0 g) was added, followed by DMF (125 mL). After thorough dispersion in DMF, the 2-Mim solution was gradually added to the LTA@ZnO solution. Additionally, a 1.0 M aqueous solution of $NaNO_3$ (100 mL) was introduced, and the setup was heated to 100 °C with a condenser fitted. The reaction proceeded for 2 days for LTA100@ZIF-8 and 4 days for LTA50@ZIF-8. Afterward, the particles underwent multiple cycles of centrifugation, followed by meticulous washing with fresh DMF, methanol, and deionized water.

4.5. Exchange to CaA@ZIF-8

To prepare the CaA@ZIF-8 samples, LTA@ZIF-8 (1.0 g) was dispersed in a solution consisting of a 1:1 volume ratio of deionized water to methanol supplemented with 0.5 M $Ca(NO_3)_2$ (200 mL).

https://doi.org/10.1021/jacsau.3c00680
JACS Au 2024, 4, 253−262

The mixture was stirred at 60 °C for 20 h. The resulting particles were collected via centrifugation. This ion-exchange process was meticulously repeated twice to ensure complete ion exchange. A control sample, the CaA zeolite, was synthesized using the same procedure applied to LTA particles. For both CaA@ZIF-8 and CaA samples, the particles underwent thorough washing through at least five cycles of centrifugation with deionized water to methanol (1:1 vol %) mixture. Finally, the particles were dried at 60 °C in a convection oven overnight.

4.6. Synthesis of 6FDA-DAM

The synthesis of 6FDA-DAM polyimide followed a previously established method.[53] This synthesis consists of two key steps: formation of poly(amic acid) and subsequent chemical imidization. In a round-bottom flask, under an inert atmosphere of argon (Ar), DAM was dissolved in NMP. While the temperature was maintained at 0 °C using an ice bath, 6FDA was slowly added. Then, the condensation reaction proceeded for 24 h, during which the solution's viscosity gradually increased. For the chemical imidization step, β-picoline and Ac_2O were introduced into the solution and stirred for an additional 24 h at room temperature. The resulting product was precipitated, washed with methanol, and subsequently dried under vacuum conditions at 210 °C overnight.

4.7. Fabrication of Mixed-Matrix Membranes

Solution casting techniques were employed to prepare dense films. For example, to prepare a membrane with 20 wt % filler loading, CaA@ZIF-8 (CaA and ZIF-8 for control membranes) (0.2 g) were dispersed in DCM (2.5 g) with the assistance of horn-type sonication (BKUP-250 K). Subsequently, the polymer was added to the dispersed solution while stirring. The mixture was further stirred overnight to obtain a homogeneous solution. After stabilizing the solution under static conditions, the dope solution was poured onto a glass plate in a glovebag saturated with DCM vapor and cast using a casting knife. The nascent membrane cast on the glass plate was immediately covered with a bridged glass plate cover to prevent rapid evaporation of DCM, leaving it in the glovebag for at least 1 h. The thickness of the resulting membranes typically ranged from 30 to 40 μm. Finally, the membrane was annealed at 220 °C for 24 h in a vacuum oven before gas permeation testing.

4.8. Characterizations

Field-emission scanning electron microscopy (FE-SEM, SU8230) and transmission electron microscopy (TEM, Talos F200X) were utilized to examine the structural morphologies of the obtained materials. Prior to FE-SEM examination, all samples, except for the zeolite, were coated with platinum at 5 mA for 100 s. Elemental analysis of the zeolite materials was conducted using an energy-dispersive X-ray spectrometer (EDS) attached to the SEM. Thermal gravimetric analysis (TGA, TG209 F1 Libra) was performed under a continuous flow of N_2. The analysis was carried out in two steps: initially rising from 30 to 250 °C at a rate of 10 °C min^{-1}, followed by maintaining the temperature at 250 °C for 30 min, and then heating at a rate of 10 °C min^{-1} from 250 to 1000 °C. Pore characteristics were investigated through N_2 physisorption at 77 K (ASAP2020). Prior to this test, the samples were activated by degassing at 220 °C for 24 h under vacuum. The CO_2 and CH_4 adsorption isotherm curves were obtained at 25 °C by using a volumetric gas adsorption analyzer (iSorbHP1 and ASAP2460).

4.9. Gas Permeation Test

The gas permeation test was conducted following the method described in our previous work.[54] Gas permeability measurements were carried out using a custom-made cell system equipped with gas chromatography (GC, YL6500). The test gas employed was a CO_2/CH_4 (50:50) binary mixture, and the operating conditions were set at 25 °C and 1 bar. Downstream of the permeation cell, helium (He) was used as a sweep gas, and the composition of the permeate gas, containing CO_2 and CH_4, was analyzed via a thermal conductivity detector (TCD). The gas permeability of individual components was determined by using eq 1

$$P_i = \frac{Q_i \cdot l}{A \cdot \Delta P_i} \tag{1}$$

Here, P_i represents the gas permeability of component i, Q_i is the molar flow rate of the permeate gas, l is the membrane thickness, A is the permeation area, and ΔP_i is the difference in partial pressure between the feed and the permeate for component i.

Subsequently, the CO_2/CH_4 selectivity was calculated from the concentration ratio of each CO_2 and CH_4 gas in the feed and permeate, as shown in eq 2

$$\alpha_{CO_2/CH_4} = \frac{y_{CO_{2,p}}/y_{N_{2,p}}}{y_{CO_{2,f}}/y_{N_{2,f}}} \tag{2}$$

Here, $y_{i,f}$ and $y_{i,p}$ represent the molar fractions of component i in the feed and permeate, respectively. The permeation testing was conducted with at least three different samples for each membrane to ensure reproducibility.

■ ASSOCIATED CONTENT

Supporting Information

The Supporting Information is available free of charge at https://pubs.acs.org/doi/10.1021/jacsau.3c00680.

Characterization data (SEM, TGA, XRD, EDS, pore size distribution, mechanical properties) and gas permeation properties (PDF)

■ AUTHOR INFORMATION

Corresponding Author

Tae-Hyun Bae − *Department of Chemical and Biomolecular Engineering, Korea Advanced Institute of Science and Technology, Daejeon 34141, Republic of Korea;* orcid.org/0000-0003-0033-2526; Email: thbae@kaist.ac.kr

Authors

Hye Leen Choi − *Department of Chemical and Biomolecular Engineering, Korea Advanced Institute of Science and Technology, Daejeon 34141, Republic of Korea;* orcid.org/0000-0002-8230-327X

Yeanah Jeong − *Department of Chemical and Biomolecular Engineering, Korea Advanced Institute of Science and Technology, Daejeon 34141, Republic of Korea*

Hongju Lee − *Department of Chemical and Biomolecular Engineering, Korea Advanced Institute of Science and Technology, Daejeon 34141, Republic of Korea*

Complete contact information is available at: https://pubs.acs.org/10.1021/jacsau.3c00680

Author Contributions

H.L.C. data curation, investigation, formal analysis, and writing—original draft; Y.J. data curation and investigation; H.L. formal analysis and investigation; T.-H.B. conceptualization, funding acquisition, project administration, supervision, and writing—review and editing. CRediT: **Hye Leen Choi** data curation, formal analysis, investigation, writing-original draft; **Yeanah Jeong** data curation, investigation; **Hongju Lee** formal analysis, investigation; **Tae-Hyun Bae** conceptualization, funding acquisition, project administration, supervision, writing-review & editing.

Notes

The authors declare no competing financial interest.

https://doi.org/10.1021/jacsau.3c00680
JACS Au 2024, 4, 253−262

■ ACKNOWLEDGMENTS

This work was supported by the National Research Foundation of Korea (NRF) grant funded by the Korean government MSIT (reference numbers: NRF-2021R1A2C3008570 and NRF- 2021M313A1084977). The authors also acknowledge the financial support by the Saudi Aramco-KAIST CO_2 Management Center.

■ REFERENCES

(1) Schuur, E. A. G.; McGuire, A. D.; Schädel, C.; Grosse, G.; Harden, J. W.; Hayes, D. J.; Hugelius, G.; Koven, C. D.; Kuhry, P.; Lawrence, D. M.; et al. Climate change and the permafrost carbon feedback. *Nature* **2015**, *520*, 171−179.
(2) Olajire, A. A. CO2 capture and separation technologies for end-of-pipe applications−A review. *Energy* **2010**, *35*, 2610−2628.
(3) Khalilpour, R.; Mumford, K.; Zhai, H.; Abbas, A.; Stevens, G.; Rubin, E. S. Membrane-based carbon capture from flue gas: a review. *J. Cleaner Prod.* **2015**, *103*, 286−300.
(4) Basu, S.; Khan, A. L.; Cano-Odena, A.; Liu, C.; Vankelecom, I. F. Membrane-based technologies for biogas separations. *Chem. Soc. Rev.* **2010**, *39*, 750−768.
(5) Castro-Muñoz, R.; Fila, V.; Martin-Gil, V.; Muller, C. Enhanced CO2 permeability in Matrimid 5218 mixed matrix membranes for separating binary CO2/CH4 mixtures. *Sep. Purif. Technol.* **2019**, *210*, 553−562.
(6) Samarasinghe, S.; Chuah, C. Y.; Yang, Y.; Bae, T.-H. Tailoring CO2/CH4 separation properties of mixed-matrix membranes via combined use of two-and three-dimensional metal-organic frameworks. *J. Membr. Sci.* **2018**, *557*, 30−37.
(7) Gong, H.; Chuah, C. Y.; Yang, Y.; Bae, T.-H. High performance composite membranes comprising Zn (pyrz) 2 (SiF6) nanocrystals for CO2/CH4 separation. *J. Ind. Eng. Chem.* **2018**, *60*, 279−285.
(8) Ordonez, M. J. C.; Balkus, K. J., Jr; Ferraris, J. P.; Musselman, I. H. Molecular sieving realized with ZIF-8/Matrimid mixed-matrix membranes. *J. Membr. Sci.* **2010**, *361*, 28−37.
(9) Li, W.; Samarasinghe, S. A. S. C.; Bae, T.-H. Enhancing CO2/CH4 separation performance and mechanical strength of mixed-matrix membrane via combined use of graphene oxide and ZIF-8. *J. Ind. Eng. Chem.* **2018**, *67*, 156−163.
(10) Mofarahi, M.; Gholipour, F. Gas adsorption separation of CO2/CH4 system using zeolite 5A. *Microporous Mesoporous Mater.* **2014**, *200*, 1−10.
(11) Adams, R. T.; Lee, J. S.; Bae, T.-H.; Ward, J. K.; Johnson, J.; Jones, C. W.; Nair, S.; Koros, W. J. CO2−CH4 permeation in high zeolite 4A loading mixed matrix membranes. *J. Membr. Sci.* **2011**, *367*, 197−203.
(12) Goh, K.; Karahan, H. E.; Yang, E.; Bae, T.-H. Graphene-based membranes for CO2/CH4 separation: Key challenges and perspectives. *Appl. Sci.* **2019**, *9*, No. 2784, DOI: 10.3390/app9142784.
(13) Yang, Y.; Chuah, C. Y.; Nie, L.; Bae, T.-H. Enhancing the mechanical strength and CO2/CH4 separation performance of polymeric membranes by incorporating amine-appended porous polymers. *J. Membr. Sci.* **2019**, *569*, 149−156.
(14) Chung, T.-S.; Jiang, L. Y.; Li, Y.; Kulprathipanja, S. Mixed matrix membranes (MMMs) comprising organic polymers with dispersed inorganic fillers for gas separation. *Prog. Polym. Sci.* **2007**, *32*, 483−507.
(15) Husain, S.; Koros, W. J. Mixed matrix hollow fiber membranes made with modified HSSZ-13 zeolite in polyetherimide polymer matrix for gas separation. *J. Membr. Sci.* **2007**, *288*, 195−207.
(16) Husain, S.; Koros, W. J. A general strategy for adhesion enhancement in polymeric composites by formation of nano-structured particle surfaces. *J. Phys. Chem. C* **2007**, *111*, 652−657, DOI: 10.1021/jp065711j.
(17) Amooghin, A. E.; Omidkhah, M.; Kargari, A. The effects of aminosilane grafting on NaY zeolite−Matrimid 5218 mixed matrix membranes for CO2/CH4 separation. *J. Membr. Sci.* **2015**, *490*, 364−379, DOI: 10.1016/j.memsci.2015.04.070.
(18) Li, W.; Zhang, Y.; Li, Q.; Zhang, G. Metal− organic framework composite membranes: Synthesis and separation applications. *Chem. Eng. J.* **2015**, *135*, 232−257.
(19) Sumida, K.; Rogow, D. L.; Mason, J. A.; McDonald, T. M.; Bloch, E. D.; Herm, Z. R.; Bae, T.-H.; Long, J. R. Carbon dioxide capture in metal−organic frameworks. *Chem. Rev.* **2012**, *112*, 724−781.
(20) Oh, J. W.; Cho, K. Y.; Kan, M.-Y.; Yu, H. J.; Kang, D.-Y.; Lee, J. S. High-flux mixed matrix membranes containing bimetallic zeolitic imidazole framework-8 for C3H6/C3H8 separation. *J. Membr. Sci.* **2020**, *596*, No. 117735.
(21) Kudasheva, A.; Sorribas, S.; Zornoza, B.; Téllez, C.; Coronas, J. Pervaporation of water/ethanol mixtures through polyimide based mixed matrix membranes containing ZIF-8, ordered mesoporous silica and ZIF-8-silica core-shell spheres. *J. Chem. Technol. Biotechnol.* **2015**, *90*, 669−677.
(22) Sorribas, S.; Zornoza, B.; Téllez, C.; Coronas, J. Mixed matrix membranes comprising silica-(ZIF-8) core−shell spheres with ordered meso−microporosity for natural-and bio-gas upgrading. *J. Membr. Sci.* **2014**, *452*, 184−192.
(23) Castarlenas, S.; Téllez, C.; Coronas, J. Gas separation with mixed matrix membranes obtained from MOF UiO-66-graphite oxide hybrids. *J. Membr. Sci.* **2017**, *526*, 205−211.
(24) Lin, R.; Ge, L.; Liu, S.; Rudolph, V.; Zhu, Z. Mixed-matrix membranes with metal−organic framework-decorated CNT fillers for efficient CO2 separation. *ACS Appl. Mater. Interfaces* **2015**, *7*, 14750−14757.
(25) Liu, Y.; Wu, C.; Zhou, Z.; Liu, W.; Guo, H.; Zhang, B. Upgrading CO2/CH4 separation performances of Pebax-based mixed-matrix membranes incorporated with core/shell-structured ZIF-L (Co)@ ZIF-8 composite nanosheets. *J. Membr. Sci.* **2022**, *659*, No. 120787.
(26) Li, H.; Zhuang, S.; Zhao, B.; Yu, Y.; Liu, Y. Visualization of the gas permeation in core−shell MOF/Polyimide mixed matrix membranes and structural optimization based on finite element equivalent simulation. *Sep. Purif. Technol.* **2023**, *305*, No. 122504.
(27) Al-Naddaf, Q.; Thakkar, H.; Rezaei, F. Novel zeolite-5A@ MOF-74 composite adsorbents with core−shell structure for H2 purification. *ACS Appl. Mater. Interfaces* **2018**, *10*, 29656−29666.
(28) Al-Naddaf, Q.; Rownaghi, A. A.; Rezaei, F. Multicomponent adsorptive separation of CO2, CO, CH4, N2, and H2 over core-shell zeolite-5A@ MOF-74 composite adsorbents. *Chem. Eng. J.* **2020**, *384*, No. 123251.
(29) Tate, K. L.; Li, S.; Yu, M.; Carreon, M. A. Zeolite adsorbent-MOF layered nanovalves for CH 4 storage. *Adsorption* **2017**, *23*, 19−24.
(30) Gong, H.; Lee, S. S.; Bae, T.-H. Mixed-matrix membranes containing inorganically surface-modified 5A zeolite for enhanced CO2/CH4 separation. *Microporous Mesoporous Mater.* **2017**, *237*, 82−89.
(31) Schejn, A.; Balan, L.; Falk, V.; Aranda, L.; Medjahdi, G.; Schneider, R. Controlling ZIF-8 nano-and microcrystal formation and reactivity through zinc salt variations. *CrystEngComm* **2014**, *16*, 4493−4500.
(32) Yang, S.; Xia, N.; Li, M.; Liu, P.; Wang, Y.; Qu, L. Facile synthesis of a zeolitic imidazolate framework-8 with reduced graphene oxide hybrid material as an efficient electrocatalyst for nonenzymatic H2O2 sensing. *RSC Adv.* **2019**, *9*, 15217−15223.
(33) Zhong, S.; Wang, Q.; Cao, D. ZIF-derived nitrogen-doped porous carbons for Xe adsorption and separation. *Sci. Rep.* **2016**, *6*, No. 21295.
(34) Bae, T.-H.; Liu, J.; Lee, J. S.; Koros, W. J.; Jones, C. W.; Nair, S. Facile high-yield solvothermal deposition of inorganic nanostructures on zeolite crystals for mixed matrix membrane fabrication. *J. Am. Chem. Soc.* **2009**, *131*, 14662−14663.
(35) Bae, T.-H.; Liu, J.; Thompson, J. A.; Koros, W. J.; Jones, C. W.; Nair, S. Solvothermal deposition and characterization of magnesium hydroxide nanostructures on zeolite crystals. *Microporous Mesoporous Mater.* **2011**, *139*, 120−129.

(36) Song, Q.; Nataraj, S.; Roussenova, M. V.; Tan, J. C.; Hughes, D. J.; Li, W.; Bourgoin, P.; Alam, M. A.; Cheetham, A. K.; Al-Muhtaseb, S. A.; Sivaniah, E. Zeolitic imidazolate framework (ZIF-8) based polymer nanocomposite membranes for gas separation. *Energy Environ. Sci.* **2012**, *5*, 8359−8369.
(37) Bux, H.; Liang, F.; Li, Y.; Cravillon, J.; Wiebcke, M.; Caro, Jr. Zeolitic imidazolate framework membrane with molecular sieving properties by microwave-assisted solvothermal synthesis. *J. Am. Chem. Soc.* **2009**, *131*, 16000−16001.
(38) Chuah, C. Y.; Goh, K.; Yang, Y.; Gong, H.; Li, W.; Karahan, H. E.; Guiver, M. D.; Wang, R.; Bae, T.-H. Harnessing filler materials for enhancing biogas separation membranes. *Chem. Rev.* **2018**, *118*, 8655−8769.
(39) Yang, Y.; Goh, K.; Weerachanchai, P.; Bae, T.-H. 3D covalent organic framework for morphologically induced high-performance membranes with strong resistance toward physical aging. *J. Membr. Sci.* **2019**, *574*, 235−242.
(40) Wang, Z.; Yuan, J.; Li, R.; Zhu, H.; Duan, J.; Guo, Y.; Liu, G.; Jin, W. ZIF-301 MOF/6FDA-DAM polyimide mixed-matrix membranes for CO2/CH4 separation. *Sep. Purif. Technol.* **2021**, *264*, No. 118431.
(41) Ahmad, M. Z.; Peters, T. A.; Konnertz, N. M.; Visser, T.; Téllez, C.; Coronas, J.; Fila, V.; de Vos, W. M.; Benes, N. E. High-pressure CO2/CH4 separation of Zr-MOFs based mixed matrix membranes. *Sep. Purif. Technol.* **2020**, *230*, No. 115858.
(42) Krokidas, P.; Spera, M. B.; Boutsika, L. G.; Bratsos, I.; Charalambopoulou, G.; Economou, I. G.; Steriotis, T. Nano-engineered ZIF fillers for mixed matrix membranes with enhanced CO2/CH4 selectivity. *Sep. Purif. Technol.* **2023**, *307*, No. 122737, DOI: 10.1016/j.seppur.2022.122737.
(43) Bae, T. H.; Lee, J. S.; Qiu, W.; Koros, W. J.; Jones, C. W.; Nair, S. A high-performance gas-separation membrane containing submicrometer-sized metal−organic framework crystals. *Angew. Chem. Int. Ed.* **2010**, *49*, 9863−9866.
(44) Bachman, J. E.; Long, J. R. Plasticization-resistant Ni2(dobdc)/polyimide composite membranes for the removal of CO2 from natural gas. *Energy Environ. Sci.* **2016**, *9*, 2031−2036.
(45) Boroglu, M. S.; Yumru, A. B. Gas separation performance of 6FDA-DAM-ZIF-11 mixed-matrix membranes for H2/CH4 and CO2/CH4 separation. *Sep. Purif. Technol.* **2017**, *173*, 269−279, DOI: 10.1016/j.seppur.2016.09.037.
(46) Liu, G.; Labreche, Y.; Chernikova, V.; Shekhah, O.; Zhang, C.; Belmabkhout, Y.; Eddaoudi, M.; Koros, W. J. Zeolite-like MOF nanocrystals incorporated 6FDA-polyimide mixed-matrix membranes for CO2/CH4 separation. *J. Membr. Sci.* **2018**, *565*, 186−193, DOI: 10.1016/j.memsci.2018.08.031.
(47) Hua, Y.; Wang, H.; Li, Q.; Chen, G.; Liu, G.; Duan, J.; Jin, W. Highly efficient CH 4 purification by LaBTB PCP-based mixed matrix membranes. *J. Mater. Chem. A* **2018**, *6*, 599−606.
(48) Liu, T.; Zhang, R.; Huang, G.; Xie, Y.; Xie, L.-H.; Li, J.-R. Mixed matrix membranes based on soluble perfluorinated metal-organic cage and polyimide for CO2/CH4 separation. *Sep. Purif. Technol.* **2023**, *318*, No. 124006.
(49) Liu, T.; Zhang, R.; Si, G.-R.; Liu, B.; Xie, Y.; Xie, L.-H.; Li, J.-R. Molecularly Homogenized Composite Membranes Containing Solvent-Soluble Metallocavitands for CO2/CH4 Separation. *ACS Sustain. Chem. Eng.* **2022**, *10*, 13534−13544.
(50) Liu, Y.; Liu, G.; Zhang, C.; Qiu, W.; Yi, S.; Chernikova, V.; Chen, Z.; Belmabkhout, Y.; Shekhah, O.; Eddaoudi, M.; Koros, W. Enhanced CO2/CH4 separation performance of a mixed matrix membrane based on tailored MOF-polymer formulations. *Adv. Sci.* **2018**, *5*, No. 1800982.
(51) Comesaña-Gándara, B.; Chen, J.; Bezzu, C. G.; Carta, M.; Rose, I.; Ferrari, M.-C.; Esposito, E.; Fuoco, A.; Jansen, J. C.; McKeown, N. B. Redefining the Robeson upper bounds for CO2/CH4 and CO2/N2 separations using a series of ultrapermeable benzotriptycene-based polymers of intrinsic microporosity. *Energy Environ. Sci.* **2019**, *12*, 2733−2740.
(52) Top, A.; Çetinkaya, H. Zinc oxide and zinc hydroxide formation via aqueous precipitation: Effect of the preparation route and lysozyme addition. *Mater. Chem. Phys.* **2015**, *167*, 77−87.
(53) Liu, Z.; Liu, Y.; Qiu, W.; Koros, W. J. Molecularly engineered 6FDA-based polyimide membranes for sour natural gas separation. *Angew. Chem. Int. Ed.* **2020**, *59*, 14877−14883.
(54) Lee, Y.; Chuah, C. Y.; Lee, J.; Bae, T.-H. Effective functionalization of porous polymer fillers to enhance CO2/N2 separation performance of mixed-matrix membranes. *J. Membr. Sci.* **2022**, *647*, No. 120309.

https://doi.org/10.1021/jacsau.3c00680
JACS Au 2024, 4, 253−262